Title
BETA SPECTROSCOPY WITH SCINTILLATION COUNTERS

Authors
Bosch, Horacio E.
Urstein, Tauba.

Publication Date
1959-10-06

UCRL-8924

UNIVERSITY OF CALIFORNIA

Ernest O. Lawrence Radiation Laboratory

BERKELEY, CALIFORNIA

DISCLAIMER

UCRL-8924

UNIVERSITY OF CALIFORNIA
Lawrence Radiation Laboratory
Berkeley, California

Contract No. W-7405-eng-48

BETA SPECTROSCOPY WITH SCINTILLATION COUNTERS

Horacio E. Bosch and Tauba Urstein

October 6, 1959

Printed for the U. S. Atomic Energy Commission

BETA SPECTROSCOPY WITH SCINTILLATION COUNTERS

Horacio E. Bosch
Lawrence Radiation Laboratory
University of California
Berkeley, California

and

Tauba Urstein
Comision Nacional de Energia Atomica
Buenos Aires, Argentina

October 6, 1959

ABSTRACT

The possibilities of the application of scintillation counters for the detection of electrons and analysis of beta spectra are described. The figures of merit and the uses in particular cases are pointed out. The setting-up of the scintillation spectrometer and the analysis of the beta spectra of some standard sources is described. The corrections of the beta spectra for resolution and backscattering are reported. Beta-gamma coincidence measurements on Rh^{106} have been performed.

BETA SPECTROSCOPY WITH SCINTILLATION COUNTERS*

Horacio E. Bosch
Lawrence Radiation Laboratory
University of California
Berkeley, California
and
Tauba Urstein
Comision Nacional de Energia Atomica
Buenos Aires, Argentina

October 6, 1959

I. INTRODUCTION

In the past few years, a new auxiliary tool in beta spectroscopy has been used, the scintillation spectrometer.[1-8] Although this is not a high-precision instrument, one can obtain certain advantages in special cases which make it a powerful tool in nuclear spectroscopy.

The resolution of the scintillation spectrometer depends on the energy, which is not the case with most magnetic spectrometers. For the 0.624-Mev conversion peak of Ba^{137m}, the resolution of the former is about 14%, while that of the latter can be 0.1%.

The transmission in the scintillation spectrometer can be high; in certain cases it is practically 100%. The ordinary magnetic spectrometers can have a transmission up to 10%. Owing to the fact that the transmission is high, the scintillation spectrometer is convenient for the detection of weak activities. If a multichannel pulse-height analyzer is coupled with a scintillation spectrometer, the entire spectrum can be studied at the same time, thus reducing to a great extent the time required for measurement. For this reason the scintillation spectrometer is also very useful for the analysis of beta spectra associated with short-lived activities. These advantages plus the fast response (10^{-8} sec.) make this instrument a valuable tool in beta spectroscopy.

---

*This work has been done partially at the Lawrence Radiation Laboratory by one of the authors (H. E. B.) under the auspices of the U.S. Atomic Energy Commission.

†Fellow from Consejo Nacional Investigaciones; on leave from Universidad de La Plata, Argentina.

In Section II, the setting-up of the scintillation spectrometer for the analysis of the beta spectra is described. In Section III, calibrations of energy and resolution are shown. In Section IV, the analysis of beta spectra of some standard sources is described. In Section V, the corrections to the beta spectra for resolution and backscattering are reported. Section VI deals with beta-gamma coincidences, the following and Section VII with positron spectra.

II. SETTING UP A SCINTILLATION SPECTROMETER FOR ANALYSIS OF BETA SPECTRA

The scintillation spectrometer for analysis of beta spectra differs from the conventional one for gamma spectroscopy in the scintillator and its mounting.

A. Scintillator

In order to determine which crystal is appropriate to detect electrons, one must review the properties of the different crystals. Sodium Iodide (Tl activated) shows the highest luminiscent yield. The yield of anthracene is 50% of that of NaI(Tl). To use NaI(Tl) for detection of electrons, one must mount the crystal in a sealed can to avoid moisture, or alternatively, introduce both crystal and source into a vacuum chamber.

The backscattering of the electrons that impinge on the crystal is the limiting factor of this technique. When the electrons are scattered, they lose part of their energy in the crystal and then escape; so the energy recorded by the crystal is less than that of the electron. If an appreciable percentage (more than 10%) of electrons is scattered out, the spectrometer will record a greater number of low-energy pulses than the actual number of electrons of these energies, which have been completely absorbed in the crystal. As a consequence, in the Kurie plot of an allowed spectrum, an upturn will appear at low energies. For this reason, it is necessary to choose a crystal in which the fraction of the backscattered electrons is reduced.

The percentage of backscattered electrons depends on the atomic number of the constituents of the crystal and increases with increasing Z. In NaI(Tl), only 20% of the total number of electrons is absorbed completely. On the other hand, in anthracene 80 to 90% of the impinging electrons are absorbed. This is the most important reason that anthracene is used instead of NaI(Tl) for the detection of electrons, even in the case of a pure electron emitter.

Anthracene has the highest efficiency of organic scintillators. The emission spectrum extends mainly between 3700 Å and 4450 Å. The decay constant is $(2.7 \pm 0.5) \times 10^{-8}$ sec. Johnston et al. have studied the linear response of anthracene crystals at low energies; their results can be seen in Fig. 1.[1] In Table I some characteristic constants for different crystals are summarized.

B. Setting up the scintillator

In order to get the best features, one must take into account the resolution and backscattering. The first is improved by increasing the collection of photons emitted by the crystal. The backscattering effect can be reduced by different arrangements of the crystal. There is one setup in which the backscattering is reduced to a great extent: the source is sandwiched between two pieces of anthracene (Fig. 2).[2] This kind of arrangement is restricted to the detection of pure beta emitters. With another mounting system, in which the source is introduced in a well crystal, the backscattered electrons are absorbed in the walls of the well. This well crystal (Fig. 3) may be used with the source inside the well (case a) or outside (case b).[3] In order to eliminate the backscattering effect, one can introduce the source into the crystal during the crystal's growth.[4]

As in general one does not analyze pure beta emitters, the usual arrangement has the source outside the scintillator.[5] The following setup was used in the present work (Fig. 4). A 1-in.-diam by 1-cm-high anthracene crystal was introduced into an aluminum can. A lucite disk was cemented to the crystal and to the photocathode surface with Canadian balsam and silicon oil respectively. Magnesium oxide powder was introduced between the wall of the can and the crystal. The upper part of the crystal was covered with a 0.2 mg/cm^2 aluminum foil in order to optimize the light collection. Since the backscattering effect is reduced with decreasing angle of incidence of electrons, a collimator was placed between the source and the crystal.

C. Relative positions between the source, detector, and collimator.

The effect of absorption of electrons in air has been calculated. In order to study the variation of the backscattering effect as a function of the source-to-crystal distance, we have used as a reference the low-energy beta spectrum of Cs^{137} and the conversion line of Ba^{137m} (0.624 Mev).

Table I

Some characteristics of scintillators

Scintillator	Density (gm/cm^3)	Refractive Index	Maximum emission wave length (Å)	Decay constant (μ)	Yield
Sodium iodide	3.67	1.77	4100	250	100
Anthracene	1.25	1.59	4400	36	48
Trans-stilbene	1.16	1.62	4100	6	28
Xylene-terphenyl	0.86	1.50	4000	3	23
Polystyrene-tetraphenyl-butadiene	1.06	1.59	4000	3	17

The variation of the ratio of intensity of the spectrum at different energies to intensity of the conversion line has been studied as a function of the source-to-crystal distance and for different thicknesses of the collimator, which is placed 2mm away from the source. The resolution is not affected by the collimator. The best results were obtained when the source was placed at a distance of 2 cm from the detector and a diaphragm 2 mm thick and 2mm in diam. was interposed 2 to 4 mm from the source. Even though the source is placed at a distance of 2 cm from the detector, there is still an appreciable absorption by the air. If it is desired to study the shape of the spectrum the source-detector system must be introduced into a vacuum chamber.

III. CALIBRATION OF THE SPECTROMETER

In order to determine the energy of the beta spectrum, it was necessary to calibrate the instrument with standard conversion lines. Figure 5 gives the beta spectrum and conversion line from Cs^{137}. The resolution for this varies from 12% to 18%. The conversion lines from Bi^{207} of 0.976 Mev, corresponding to the transition of 1.064 Mev (K-conversion of the transition of the 1.633 Mev level) and those of 0.544 Mev and 0.477 Mev corresponding to the L and K-conversion, respectively, of transition of 0.569 Mev level, are plotted in Fig. 6. The conversion line (K + L) of 0.175 Mev from In^{114m} is plotted in Fig. 7. The experimental data and resolution of conversion lines from different authors, are in Table II.

IV. ANALYSIS OF BETA SPECTRA OF STANDARD SOURCES

Beta Spectrum of Co^{60}

The most intense component of the beta spectrum of Co^{60} has an energy of 0.319 ± 0.003 Mev and is an allowed transition.[10] The resulting spectrum is plotted in Fig. 8, and the corresponding Kurie plot is seen in Fig. 9. The mean value for the maximum energy, which was determined in a series of measurements, is 0.326 ± 0.003 Mev.

Beta Spectrum of P^{32}

A single beta transition occurs between the 1+ level of P^{32} and the 0+ level of S^{32}. The transition is allowed[11] although a forbiddenness factor was pointed out by Porter et al.[12] The characteristic beta spectrum and the corresponding Kurie plot are represented in Figs. 10 and 11, respectively.

Table II

Resolution of the standard conversion lines obtained with scintillation spectrometers by various authors.

Substance	Energy (Mev)	Resolution (%)				
		Bisi et al.[6]	Ricci[7]	Freedman et al.[8]	Johnson et al.[9]	Present authors
In^{114m}	0.175					25
Bi^{207}	0.477		16			18
Ba^{137m}	0.624	11	13	18	12.9	13.8
Bi^{207}	0.976		11			13

One can clearly see the departure from linearity down to 1 Mev. After a series of measurements, the value of 1.706 ± 0.011 Mev was assigned to the maximum energy of the beta spectrum of P^{32}. The value obtained with a magnetic spectrograph is 1.711 Mev.[12]

Beta Spectrum of Cs^{137}

As is well known, the beta spectrum of Cs^{137} is complex; a weak branch of a maximum energy of 1.18 Mev and a strong one of 0.52 Mev are the two components.[13] We have employed two sources: a weak one in which the more energetic branch cannot be observed, and a strong one in which it can be seen.

The beta spectrum of the first sample, with the conversion line of 0.624 Mev, is represented in Fig. 5. The resolution of this line is 15%. The spectrum is known to be in the unique forbidden category, as can be seen in Fig. 12(a) in the corresponding Kurie plot. This can be corrected [Fig. 12(b)] by applying the factor

$$C = (W_0 - W)^2 + (W^2 - 1).$$

The mean value for the maximum energy was determined to be 0.532 ± 0.024 Mev. The beta spectrum of the second sample of Cs^{137} is plotted in Fig. 13, where one can observe the more energetic branch.[14] The Kurie plot is represented in Fig. 14. The maximum energy of the spectrum was determined to be 1.180 ± 0.010 Mev. The contribution of the spectrum at the low-energy region is practically zero within the experimental error; therefore, it is not necessary to perform the subtraction.

Considering the areas under both the beta spectrum (S_b) and the conversion peak (S_e), we can estimate the conversion coefficient corresponding to the transition of 0.661 Mev in Ba^{137m}. This conversion coefficient can be expressed as

$$\alpha_K = \frac{N_e}{N_\gamma} = \frac{N_e}{N_b - N_e} = \frac{S_e}{S_b - S_e} .$$

The average value obtained in three measurements is $\alpha_K = 0.109 \pm 0.020$.

Tables III and IV summarize the results, and compare them with those obtained by other authors.

V. CORRECTIONS TO BE APPLIED TO THE BETA SPECTRA OBTAINED WITH SCINTILLATION SPECTROMETERS

The measured spectrum differs from the actual because of the resolution and backscattering effects. If one electron of energy E' from a monoenergetic beam impinges on an organic crystal, because of the backscattering and resolution events, it can be recorded when the discriminator channel (with window $\Delta E'$) is set at an energy $E \neq E'$. If $N(E')$ is the total intensity (per unit time) of the beam, a fraction $M(E_i)$ of the total intensity will be recorded at each position of the channel corresponding to different energies E_i. If $N(E', E_i)$ is the shape of the experimental line, the fraction $M(E_i)$ is given by

$$M(E_i) = N(E') \cdot L(E', E_i) \cdot \Delta E',$$

where we have

$$L(E', E_i) = \frac{N(E', E_i)\ \Delta E_i}{\int_0^{E_{max}} N(E', E_i)\, dE_i} .$$

Table III

Maximum energies of the standard beta spectra obtained with scintillation spectrometers by different authors.

Nuclide	Maximum energy Magnetic spectrometer (Mev)	Maximum energy, scintillation spectrometer (Mev)			
		Palmer & Laslett[15]	Ricci[7]	Bisi et al.[6]	Present authors
Cs^{137}	0.520	0.500	0.510 ±0.01		0.532 ± 0.024
Co^{60}	0.319		0.305 ±0.005	0.320	0.326 ± 0.003
P^{32}	1.711	1.86	1.695 ±0.015	1.64	1.706 ± 0.011
Cs^{137}	1.18		1.2		1.180 ± 0.010

UCRL-8924

Table IV

Internal conversion coefficient for Ba^{137m} obtained with scintillation spectrometers by various authors

Nuclide	Internal conversion coefficient		
	Magnetic spectrometer[16]	Ricci[7]	Present authors
Ba^{137m}	0.110 ± 0.022	0.114 ± 0.022	0.109 ± 0.020

The significance of the $L(E', E_i)$ function can be seen in Fig. 15 in which the coincidence spectrum between the conversion line of Ba^{137m} (0.624 Mev) and the x-rays, is plotted. In addition, the backscattering effect can be clearly seen. The fraction of the total intensity of the electrons detected at 24 v with a channel setting 2 v wide, is

$$L(0.624, E_{24}) = \frac{\text{shaded area}}{\text{total area}} .$$

When a continuous spectrum is analyzed, there is an actual distribution $N(E'_k)$ of the number of electrons per unit time as a function of the incident energy E'_k. For each setting of the discriminator channel, there is a partial contribution of each $N(E'_k)$. Then the intensity per unit time recorded at an energy E_i is the sum of all the partial contributions:

$$M(E_i) = \sum N(E'_k) \cdot L(E'_k, E_i)\, \Delta E'_k$$

$$= \int_0^{E'_{max}} N(E') \cdot L(E', E_i)\, dE' \qquad (1)$$

The intensity fraction $M(E_i)$ recorded at E_i cannot be obtained from the continuous spectrum. Freedman et al.[8] have given a method for obtaining the fraction $L(E'_k, E_i)$ from the observed experimental shape spectrum of standard sources of monoenergetic lines. We have chosen the following conversion lines:

(a) Ba^{137m} (e_K = 0.624 Mev), obtained in coincidence with the x-rays

(b) Bi^{207} (e_{K+L} = 0.499 Mev; K/L = 3.4) obtained in coincidence with the 1.064-Mev gamma ray

(c) Bi^{207} (e_{K+L} = 0.991 Mev, K/L = 4.0) obtained in coincidence with the 0.569-Mev gamma ray.

In the last two cases it was necessary to subtract the coincidence spectrum between the Compton electrons produced in the anthracene crystal by the gamma radiation and the corresponding cascading gamma ray detected in the NaI(Tl) crystal.

The experimental conversion lines, normalized to the same height, are plotted in Fig. 16. It can be observed that all the lines exhibit a constant tail. The ratio of the height of the tail to the height of the peak was measured as 0.084 (Freedman et al.[8] reported the value 0.075 ± 0.010). Once these experimental line shapes are plotted, we can draw new line shapes (every 20 kev for instance), since the variation of the shape is smooth. One obtains the variation of the peak at the base and at 1/4, 1/2, and 3/4 of the height as a function of the energy, as is seen in Fig. 17. Once the line-shapes are constructed each 20 kev according to Fig. 17, one can obtain the value for $L(E'_k, E_i)$ by taking the area under the line E'_k in one interval E_i to $E_i + \Delta E_i$, and dividing by the total area under the line, according to the definition. Once the fractions $L(E'_k, E_i)$ are determined, they have to be introduced in Eq. (1) in order to obtain the actual spectrum from the measured one. As a zeroth-order approximation to $N(E')$ one can choose $M(E)$ and obtain a new $M_1(E)$, and repeat this procedure until the desired convergence is obtained. We have used the convergence method employed by Freedman et al.[8] The first approximation to the actual spectrum is given by

$$N_1(E)\,\Delta E = M(E) - [M_1(E) - M(E)] = 2\,M(E) - M_1.$$

We have applied this correction to the beta spectrum of P^{32}. Figure 18 (a) and (b) shows respectively the difference obtained in the Kurie plot of the beta spectrum of P^{32} without and with application of the mentioned correction. Although the departure from linearity with the correction starts at 400 kev instead of 1000 kev, there is still a limitation imposed by the efficiency of the crystal and the absorption by the air.

VI. BETA-GAMMA COINCIDENCES

For the sake of completeness and as an example of the possibilities of the instrument, we have chosen to measure beta-gamma coincidences in the case of Rh^{106}. This nuclide decays to Pd^{106} by beta emission. The Kurie plot corresponding to the beta spectrum is shown in Fig. 19. The maximum energy was determined to be 3.5 Mev. With magnetic spectrometers, values of 3.52 Mev are reported.[17,18]

Beta-gamma coincidences were performed by setting the discriminator in the beta channel at 1.550 Mev. The beta rays are in coincidence with 0.513-, 0.620-, 1.050-, and 1.150-Mev gamma rays, as is shown in Fig. 20. These measurements were taken with and without 1/8-in. lead absorber in the gamma side, in order to determine how much of the 1.150-Mev gamma ray is due to solid-angle addition of 0.511- and 0.620-Mev gamma rays. The fact that a gamma ray of 1.150-Mev is in coincidence with a beta spectrum of end-point energy >1.550 Mev indicates that this gamma ray corresponds to a ground transition from the second excited level of Pd^{106}. This implies that this level has a character of 2+. As is known, the second excited state in Pd^{106} was determined to be 0+, according to angular-correlation measurements.[19] The beta-gamma-coincidence results indicate that, in addition to the 0+ level at 1.140-Mev, one has to assume the presence of a 2+ level. This confirms the results reported recently by Robinson, McGowan, and Smith on gamma-gamma coincidences from the decay of Rh^{106}.[20]

VII. ANALYSIS OF POSITRON SPECTRA

It is of interest to comment on the determination of end-point positron spectra. It seems that the contribution of Compton electrons coming from the interaction of the annihilation radiation with the crystal is unimportant.[21] This means that there is no an appreciable amount of pile-up between the light flash produced by the Compton electrons and the light flash produced in the interaction of positrons with the crystal. In order to prove this, the positron spectrum of Ge^{68} was measured, its Fermi plot being represented in Fig. 21. The average end-point energy found was 1.950 ± 0.050 Mev. This is in good agreement with previous measurements of 1.940 ± 0.050 Mev by Crasemann et al.[22]

VIII. CONCLUSIONS

Our results show the possibilities of the beta scintillation spectrometer as a tool to be used in the analysis of beta spectra.

The method described is very useful when beta radiation from short half lives or weak activities are to be examined. The accuracy in the determination of the maximum energy of the beta spectrum compared with the standard known maximum energies is within 5%. The beta spectra recorded by the scintillation spectrometer are sensitive to the degree of forbiddenness of the corresponding transitions. When the correction for backscattering is applied, one can obtain a fairly good agreement between the Kurie plot of an allowed spectrum and the same Kurie plot obtained with a magnetic spectrometer. Nevertheless, there is a limitation of the method because of the efficiency of the crystal for low energies and the absorption by air. If one is interested in the study of the shape of the beta spectrum, one has to place both source and crystal into a vaccum chamber in order to reduce the absorption effect.

No particular correction is needed for the proper determination of the end-point energy of positron spectra.

ACKNOWLEDGMENTS

One of the authors (H. E. B.) wants to acknowledge the hospitality afforded him at the Lawrence Radiation Laboratory. The authors are very much indebted to Drs. John Rasmussen, Richard Diamond, Jack Hollander, Daniel Horen, and Gaja Alaga from the Lawrence Radiation Laboratory and Drs. Melvin Freedman and Carlos Mallmann from Argonne for helpful discussion and careful reading of the manuscript. The assistance of Pilar Reyes and Lucia Lagatta in the performance of the work is deeply appreciated.

REFERENCES

1. Johnston, Birkhoff, Cheka, Hubbel, and Saunders, Rev. Sci. Instr. 28, 765 (1957).
2. B. H. Ketelle, Phys. Rev. 80, 758, (1950).
3. Physics Quarterly Progress Report for Period Ending Dec. 20, 1950 ORNL-940.
4. G. Scharff-Goldhaber, Phys. Rev. 83, 480 (1951).
5. R. C. Davis and P. R. Bell, Phys. Rev. 83, 483 (1951).
6. Bisi, Germagnoli, and Zappa, Nuovo cimento 13, 1007 (1956).
7. R. A. Ricci, Physica 23, 693 (1957).
8. Freedman, Novey, Porter, and Wagner, Rev. Sci. Instr. 27, 716 (1956).
9. Johnson, Johnson, and Langer, Phys. Rev. 102, 1142 (1956).
10. Kamada, Teranishi, and Yoshizawa, J. Phys. Soc. Japan 13, 763 (1958).
11. K. Siegbahn, Phys. Rev. 70, 127 (1946).
12. Porter, Wagner, and Freedman, Phys. Rev. 107, 135 (1957).
13. J. S. Osoba, Phys. Rev. 76, 345 (1949).
14. We have considered the axial vector interaction in order to explain the forbiddenness of this transition. The corresponding factor has the form

$$C_{2Va}\ g_v^2 \langle R_{ij} \rangle^2 \Big\{ -2/15\, q^2 N_0 - 2q N_1 + (1/12\, q^2 L_0 + 3/4\, L_1)\, \Gamma_1^2 - 2\Gamma_1 (-1/6\, q^2 N_0 - 3/2\, N_1) + 1/12\, \Gamma_2^2 (3/5\, q^3 N_0 + q^2 M_0 + 6q N_1) + 4/3\, g\, \Gamma_2 M_0 q^2 + 2g\, \Gamma_1\, \Gamma_2 (4/3\, Q_0 q^2 + 12\, Q_1) \Big\} .$$

   The formula is from E. Konopinski and G. Uhlenbeck, Phys. Rev. 60, 308 (1941); E. Greuling, Phys. Rev. 61, 568 (1942); and D. L. Pursey, Phil. Mag. 42, 1193 (1951).
15. J. Palmer and L. Laslett, Application of Scintillation Counters to Beta-Ray Spectroscopy, ISC-174, December, 1950.
16. A. H. Wapstra, Arkiv. Fysik 7, 275 (1953).
17. D. E. Alburger and B. J. Toppel, Phys. Rev. 100, 1357 (1955).
18. Grigoriev, Zolotavin, Kuzmin, and Pavlitskaia, J. Acad. Sci (USRR), Physics Section, 22, 194 (1958).
19. J. J. Kraushaar and M. Goldhaber, Phys. Rev. 89, 1081 (1953).
20. Robinson, Mc Gowan, and Smith, Bull. Am. Phys. Soc., Series II, 4, 279 (1959).
21. James Ferguson, Naval Radiological Defense Laboratory, San Francisco, Calif., private communication.
22. Crasemann, Rehfuss, and Easterday, Phys, Rev. 102, 1344 (1956).

FIGURE LEGENDS

Fig. 1. Linear response of an anthracene crystal up to 120-kev incident electrons (From Ref. 1).

Fig. 2. Setup of the source-crystal system in order to reduce the back-scattering effect.

Fig. 3. Another setup of the source and crystal to reduce the back-scattering effect by using a well crystal.

Fig. 4. Setup of source and crystal used in the present work.

Fig. 5. Low-energy bera spectrum and conversion line from Cs^{137}.

Fig. 6. Conversion lines from Bi^{207} of 0.976, 0.544, and 0.477 Mev.

Fig. 7. Conversion line (K+L) of 0.175 Mev from In^{114m}.

Fig. 8. Beta spectrum from Co^{60} after subtraction of gamma background, obtained with a single-channel analyzer.

Fig. 9. Kurie plot corresponding to the beta spectrum from Co^{60}.

Fig. 10. Beta spectrum from P^{32} obtained with a single-channel analyzer.

Fig. 11. Kurie plot corresponding to the beta spectrum from P^{32}.

Fig. 12. (a) Kurie plot for the low-energy branch of the Cs^{137} beta spectrum. (b) Linearization of the above Kurie plot with the correction factor $C = (Wo - W)^2 + W^2 - 1)$.

Fig. 13. Low- and high-energy beta spectra from Cs^{137} and conversion lines from Ba^{137m}.

Fig. 14. Kurie plot corresponding to the most energetic beta spectrum from Cs^{137}.

Fig. 15. Coincidence spectrum between the electron-conversion line and the x-rays of Ba^{137m}.

Fig. 16. Experimental line shape corresponding to monoenergetic electrons from Ba^{137m} and Bi^{207}, normalized to the same height.

Fig. 17. Width at the base and 1/4, 1/2, and 3/4 of the height of the monoenergetic lines, as a function of the energy.

Fig. 18. (a) Kurie plot corresponding to the experimental beta spectrum of P^{32}. (b) Kurie plot from beta spectrum of P^{32} when the correction for backscattering is applied.

Fig. 19. Kurie plot corresponding to the beta spectrum from Rh^{106}.

Fig. 20. Gamma spectrum in coincidence with beta rays from Rh^{106} when the discriminator is set at 1.55 Mev.

Fig. 21. Fermi plot corresponding to the positron spectrum of Ge^{68}.

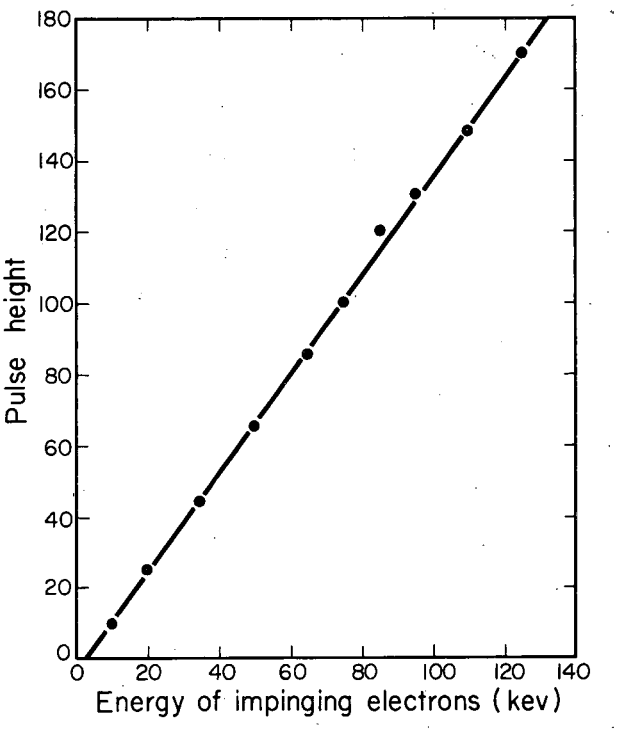
Pulse height
Energy of impinging electrons (kev)
0
20
40
60
80
100
120
140
160
180
MU-18623

Fig. 1

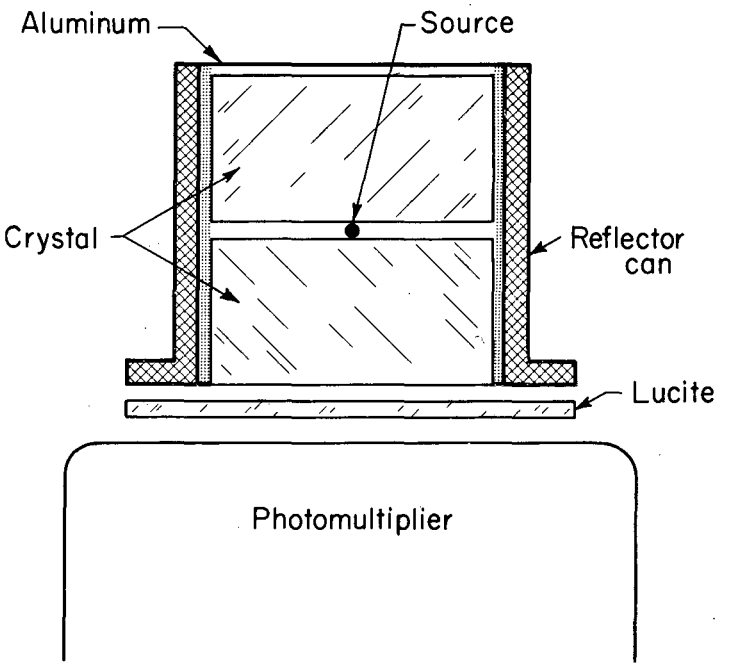
Aluminum
Source
Crystal
Reflector can
Lucite
Photomultiplier
MU-18617

Fig. 2

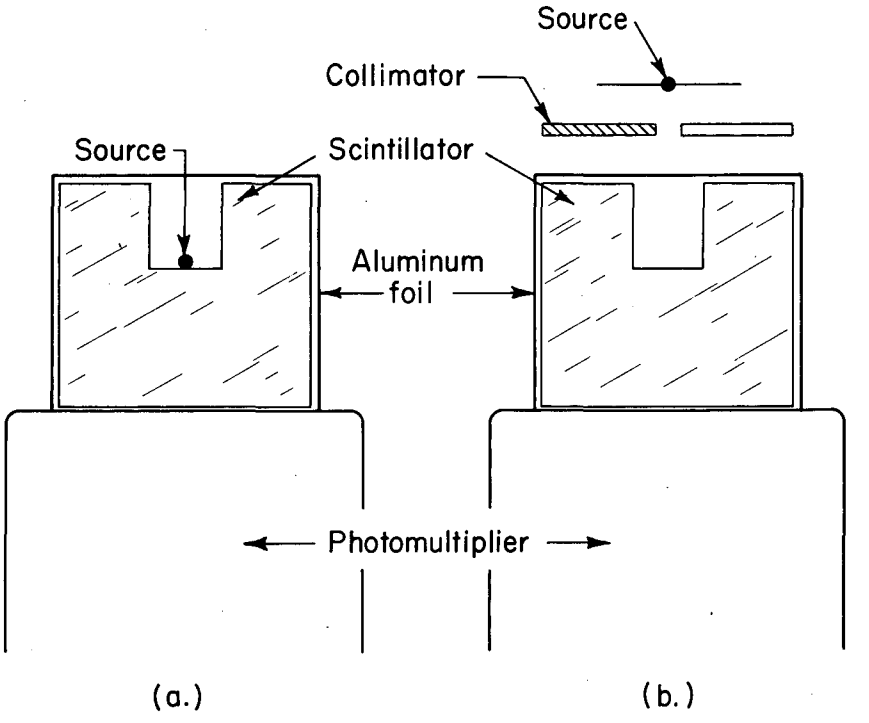
Source
Collimator
Source
Scintillator
Aluminum
foil
Photomultiplier
(a.)
(b.)
MU-18616

Fig. 3

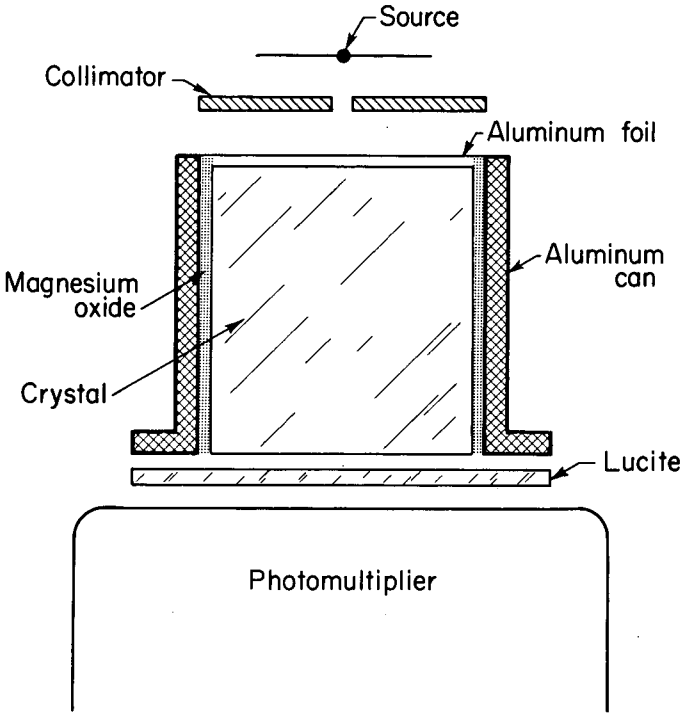
Source
Collimator
Aluminum foil
Aluminum can
Magnesium oxide
Crystal
Lucite
Photomultiplier
MU-18618

Fig. 4

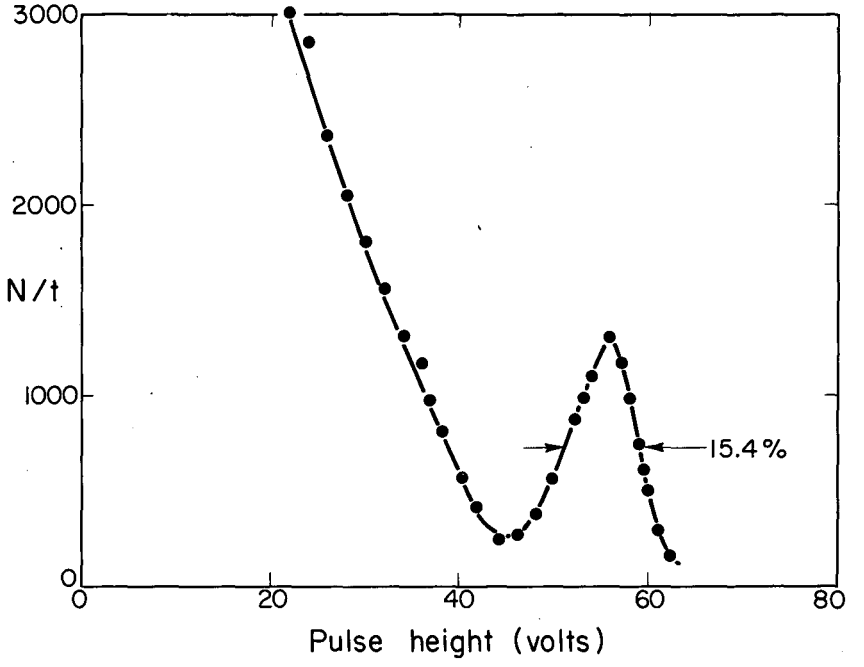
3000
2000
N/t
1000
0
0
20
40
60
80
15.4%
Pulse height (volts)
MU-18615

Fig. 5

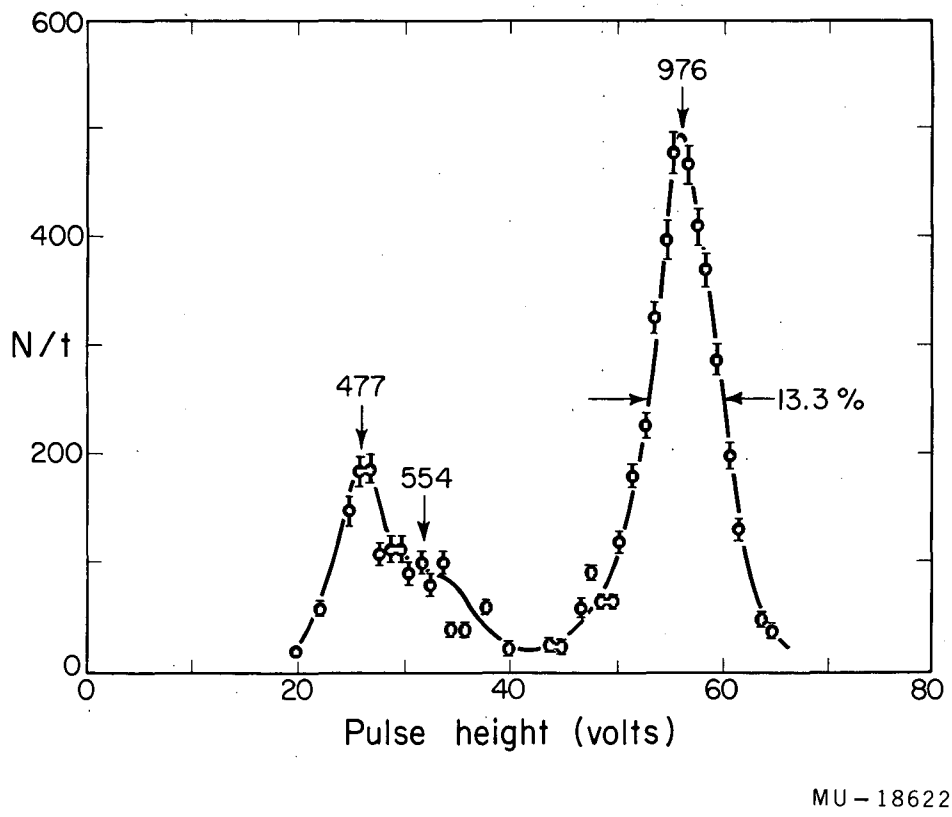
600
400
200
0
N/t
976
477
554
13.3 %
0
20
40
60
80
Pulse height (volts)
MU-18622

Fig. 6

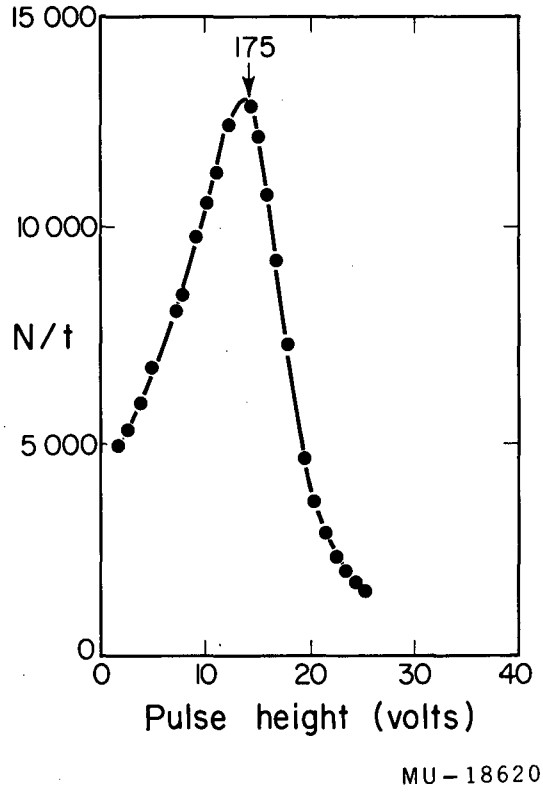
15 000
10 000
5 000
0
N/t
175
0
10
20
30
40
Pulse height (volts)
MU-18620

Fig. 7

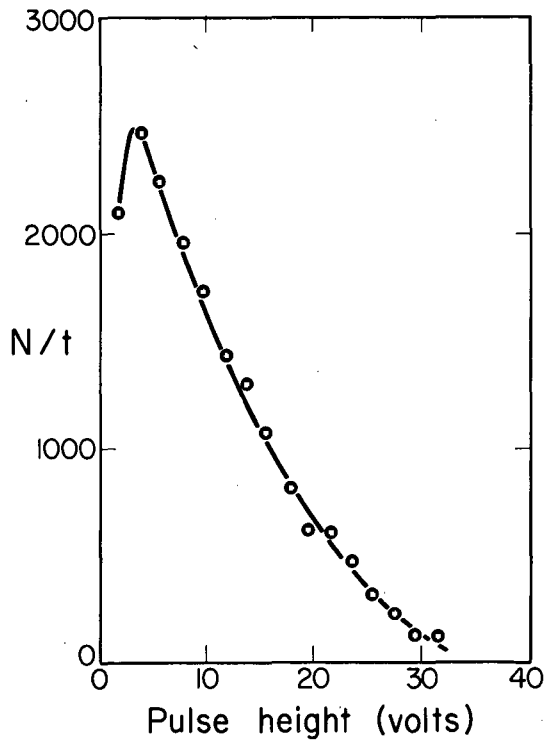

Fig. 8

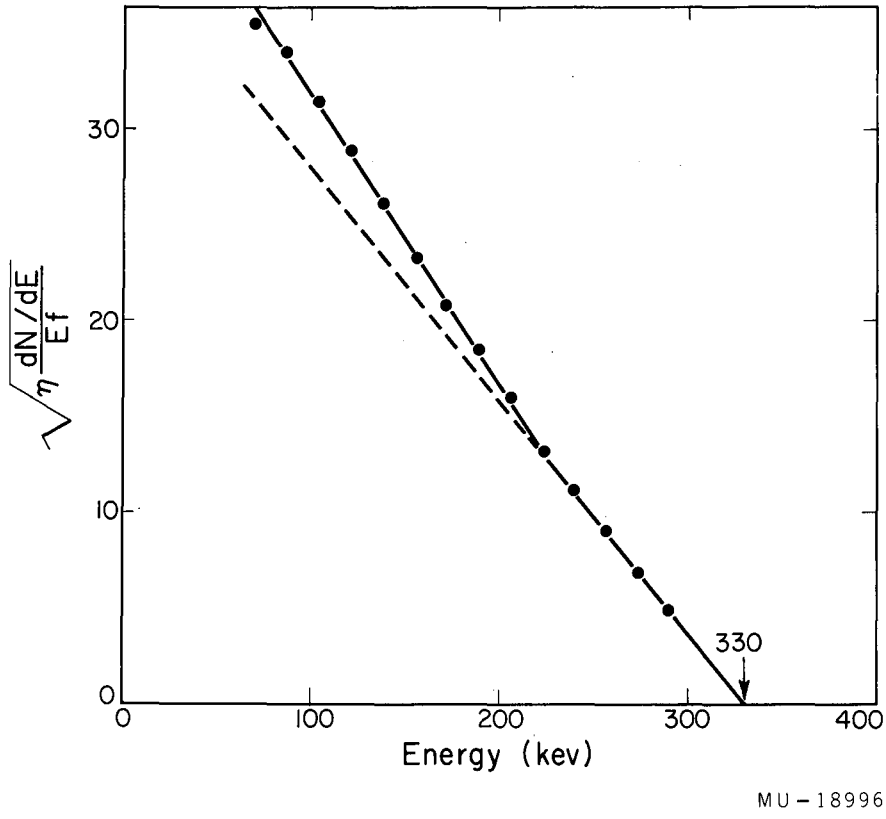
$\sqrt{\eta \frac{dN/dE}{Ef}}$
30
20
10
0
0
100
200
300
400
330
Energy (kev)
MU-18996

Fig. 9

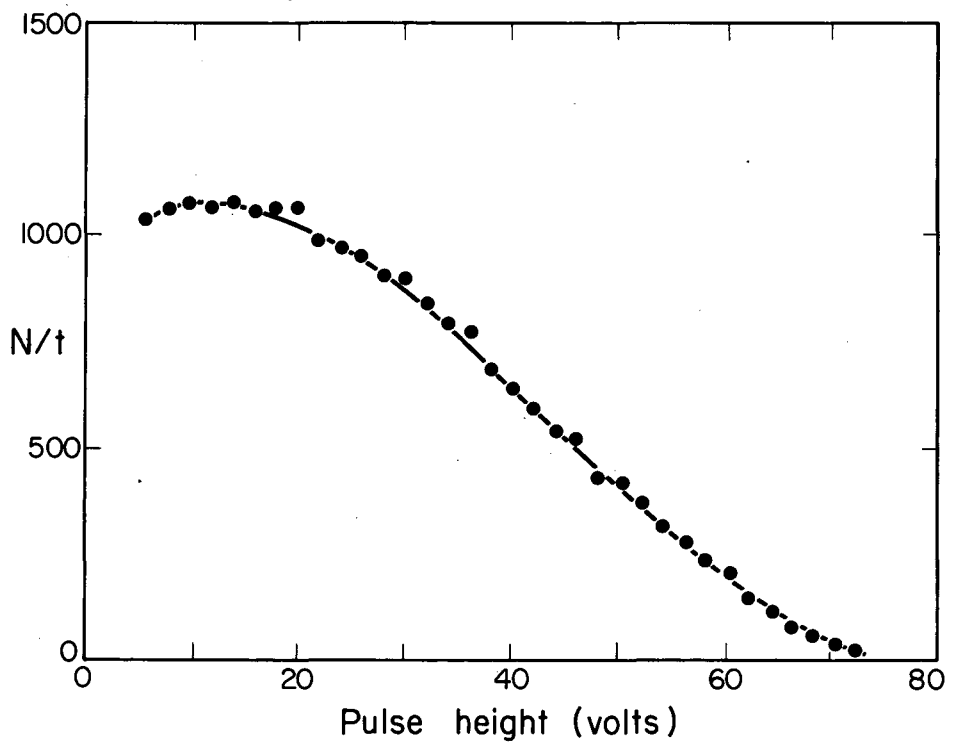

Fig. 10

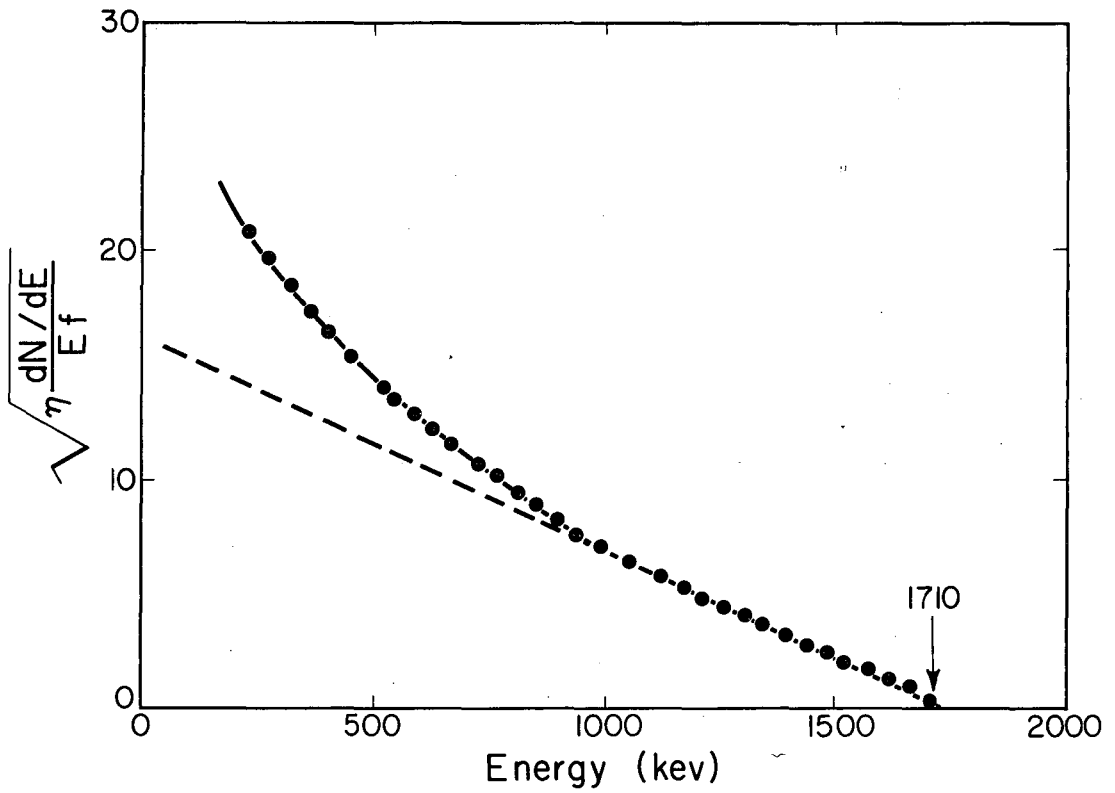
30
20
10
0
0
500
1000
1500
2000
1710
Energy (kev)
$\sqrt{\eta \frac{dN/dE}{Ef}}$
MU-18992

Fig. 11

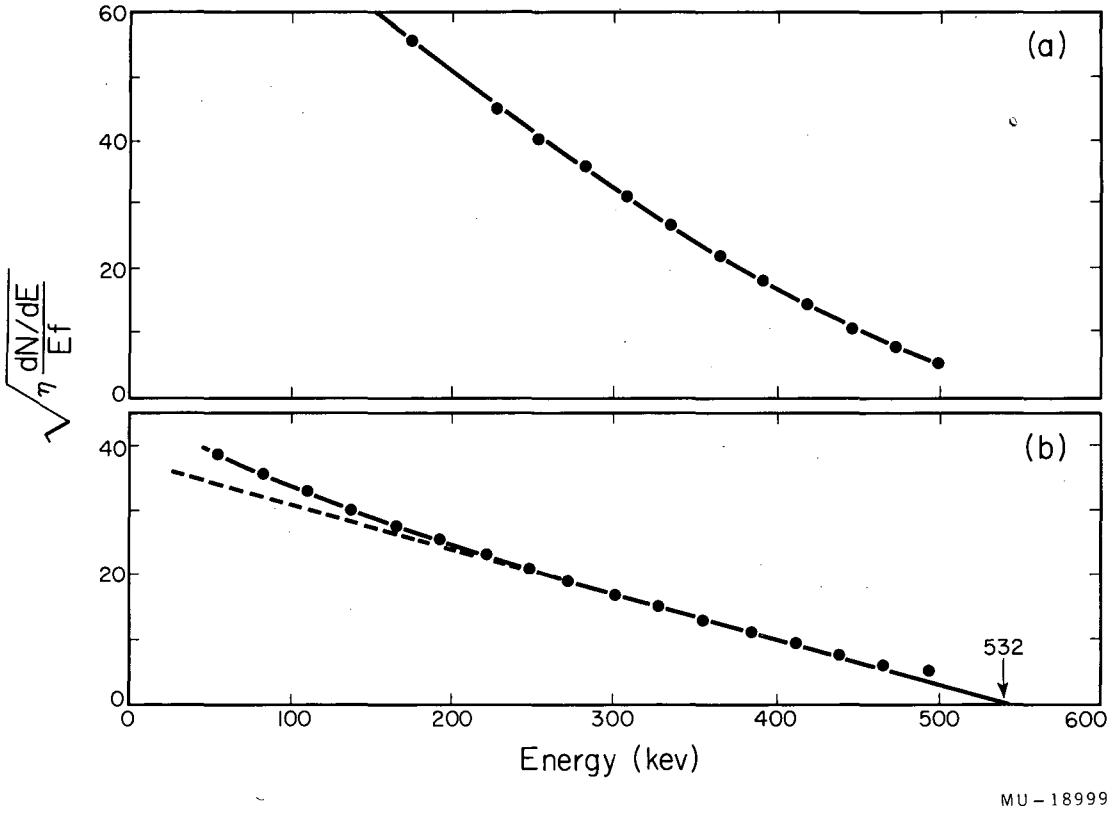
60
40
20
0
(a)
40
20
0
(b)
532
0
100
200
300
400
500
600
Energy (kev)
$\sqrt{\eta \frac{dN/dE}{Ef}}$
MU-18999

Fig. 12

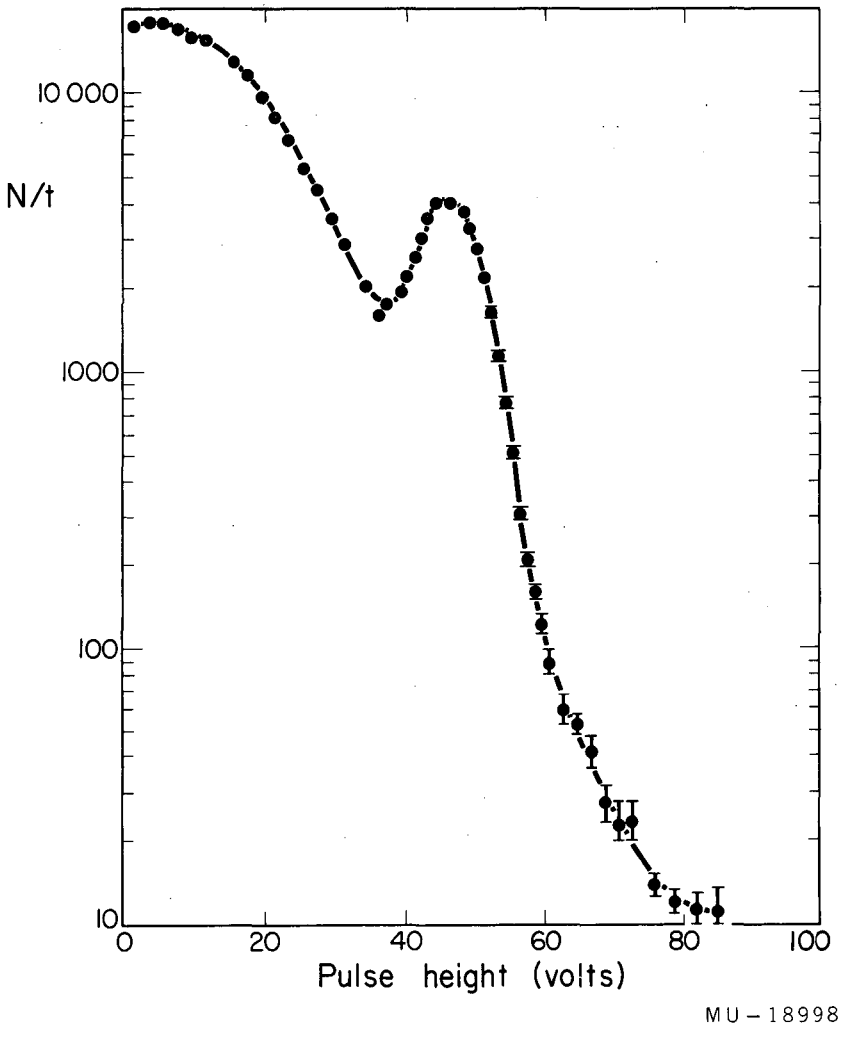
10 000
1000
100
10
N/t
0
20
40
60
80
100
Pulse height (volts)
MU-18998

Fig. 13

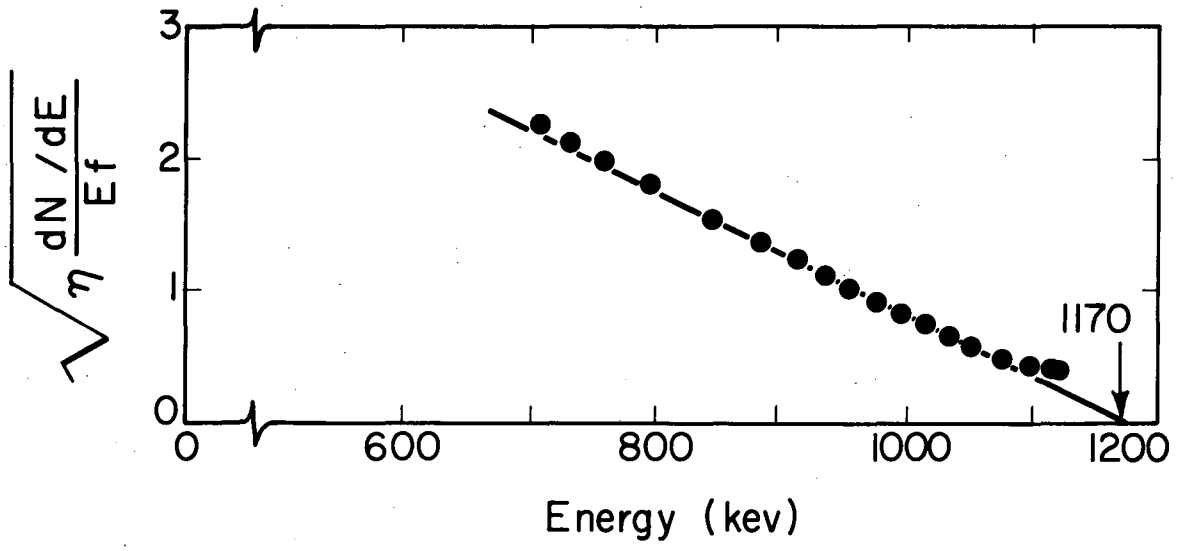

MU-18994

Fig. 14

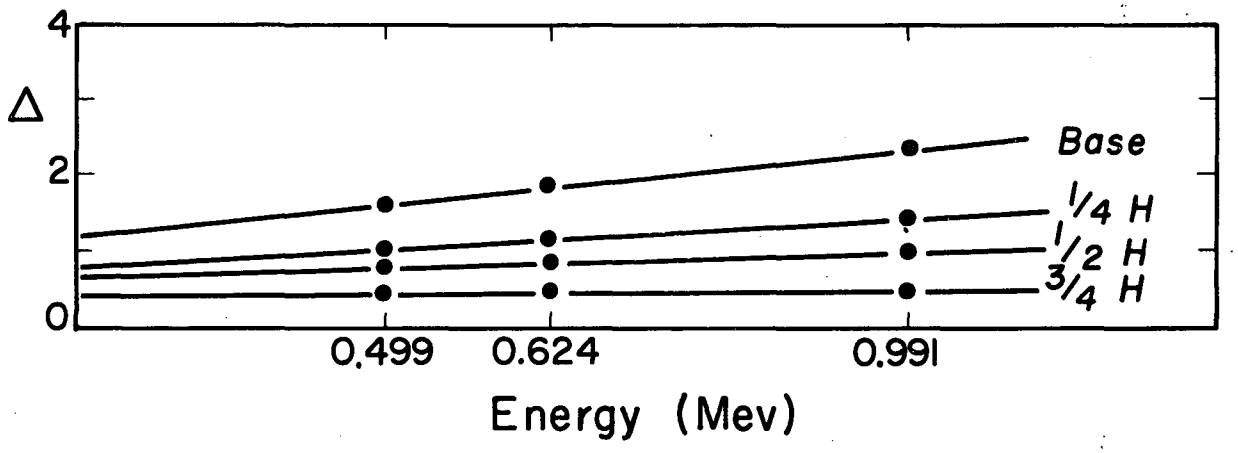

MU-18993

Fig. 17

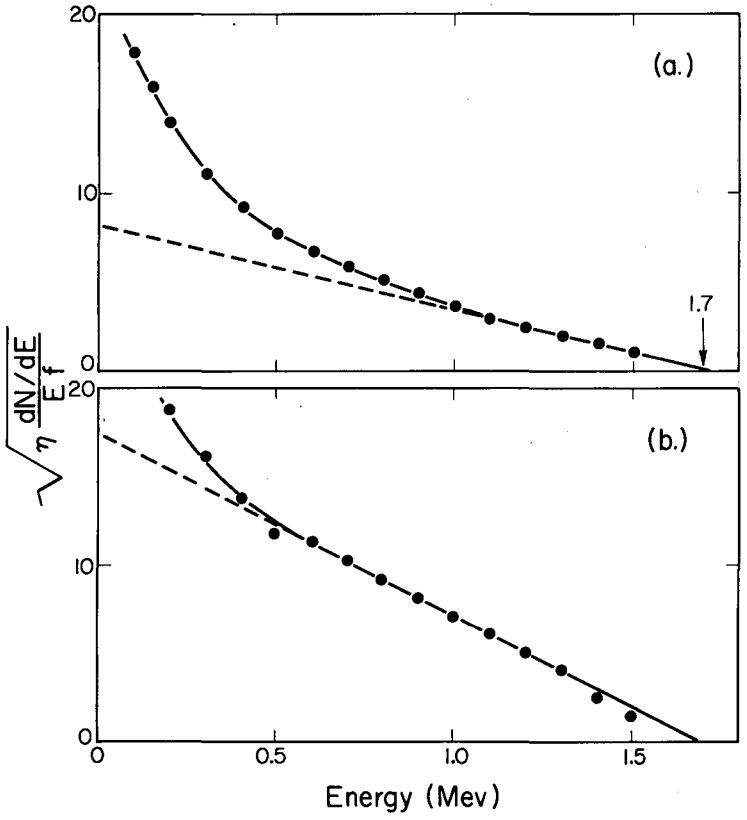
20
10
0
(a.)
1.7
20
10
0
(b.)
0
0.5
1.0
1.5
Energy (Mev)
$\sqrt{\eta \frac{dN/dE}{Ef}}$
MU-18624

Fig. 18

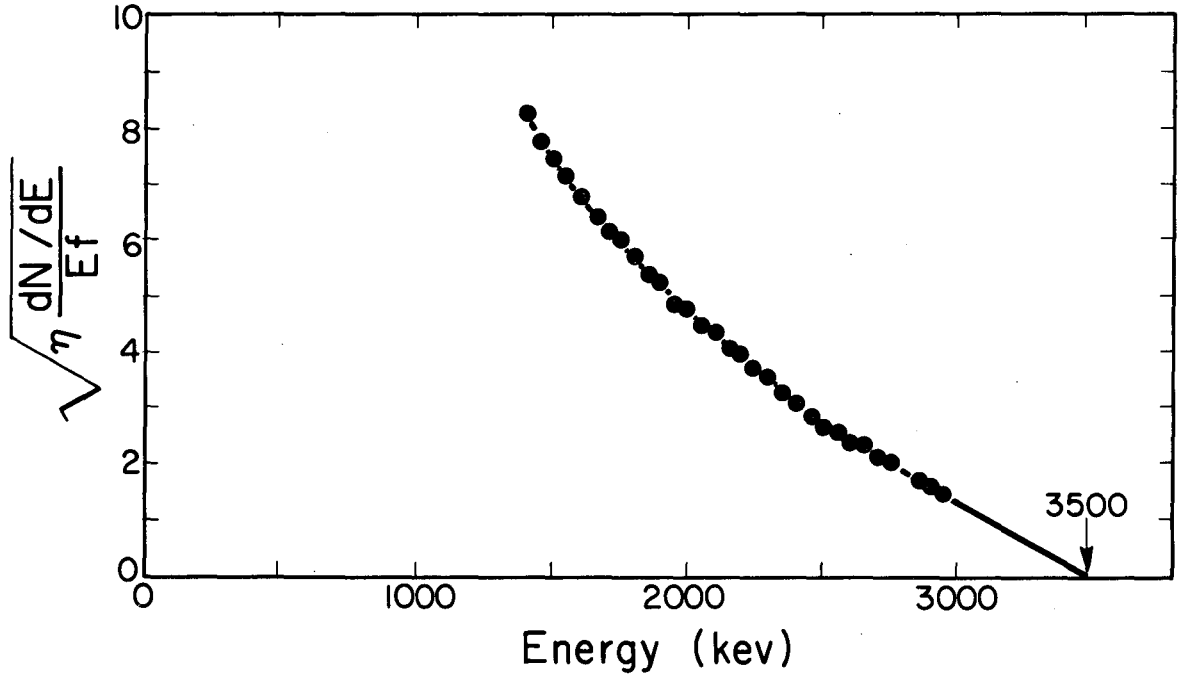

MU-18995

Fig. 19

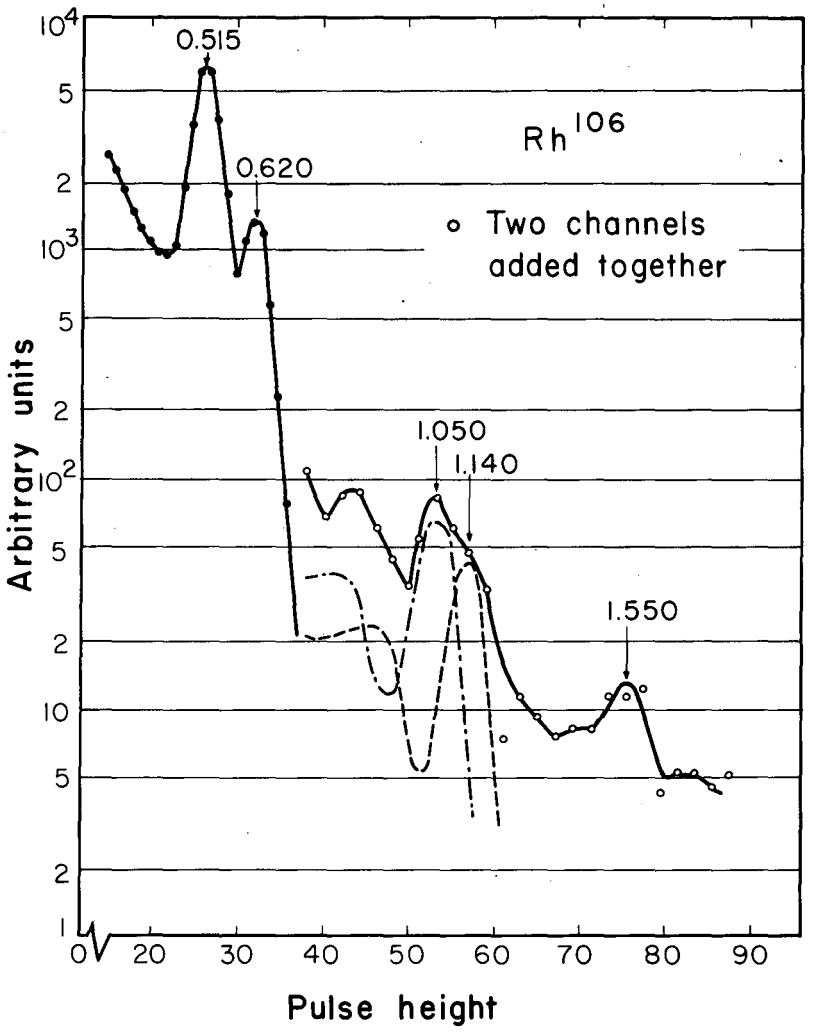
0.515
0.620
Rh 106
Two channels added together
1.050
1.140
1.550
Arbitrary units
Pulse height
MU-18951

Fig. 20

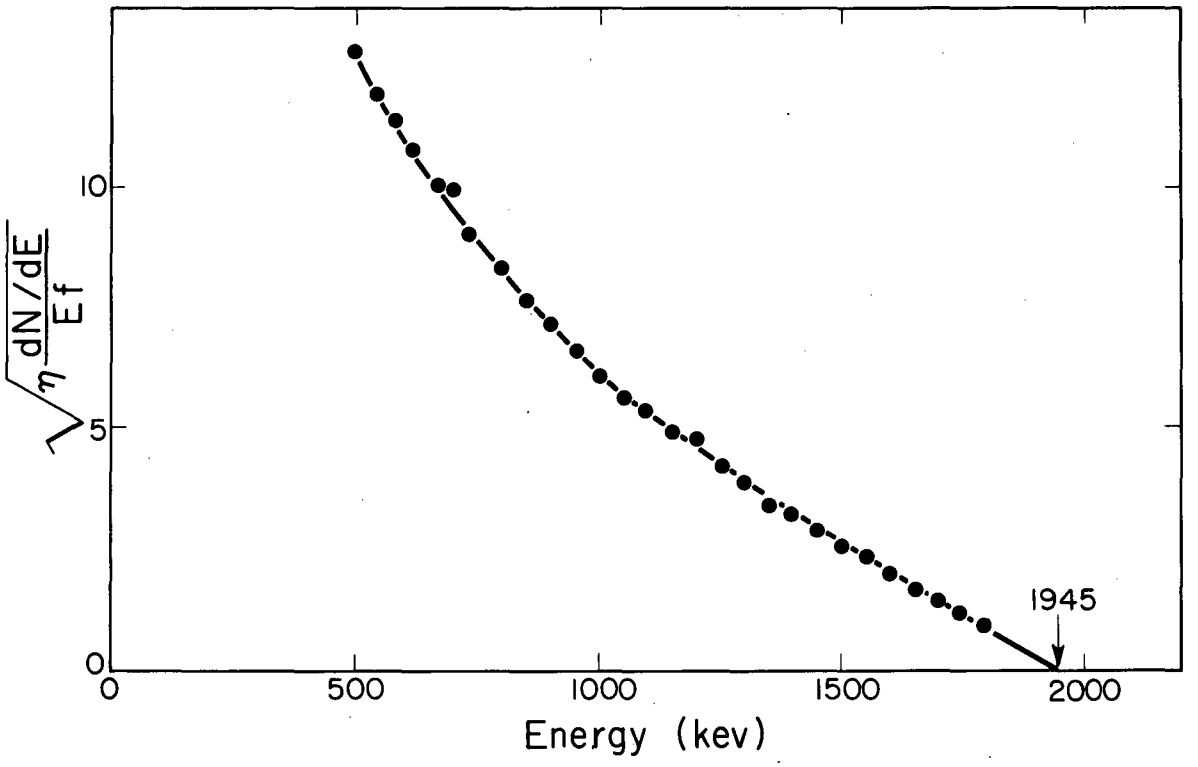
$\sqrt{\eta \frac{dN/dE}{Ef}}$
10
5
0
0
500
1000
1500
2000
1945
Energy (kev)
MU-18997

Fig. 21